Computation of the Dynamic Axial Modulus and Activation Potential of Virtual Self-Healing Asphalt Mixtures with Encapsulated Rejuvenators

Angelica Viana-Sepulveda[1], Silvia Caro[1*], Daniel Castillo[2] and Jose Norambuena-Contreras[3]

[1] Department of Civil and Environmental Engineering, Universidad de los Andes, Bogotá, Colombia; am.viana10@uniandes.edu.co (A.V.-S.); scaro@uniandes.edu.co (S.C.)
[2] Department of Civil Engineering, Michigan State University, Michigan, United States; casti245@msu.edu (D. C.)
[3] Materials and Manufacturing Research Institute, Department of Civil Engineering, Faculty of Science and Engineering, Swansea University, Bay Campus, SA1 8EN, UK; jnorambuena@ubiobio.cl (J.N.-C.)

*Corresponding author: scaro@uniandes.edu.co (S.C.)

Abstract

Integrating encapsulated rejuvenators into asphalt mixtures is an emerging technology aimed at enhancing the self-healing capabilities of asphalt mixtures. The healing process occurs when liquid agents are released from biopolymeric capsules and improve the intrinsic healing capacity of the asphalt binder. The effectiveness of this technology requires that: i) the addition of capsules does not compromise the mechanical performance of the asphalt mixture, ii) a minimum number of capsules will activate (i.e., start to release the healing agent), and iii) the released agent efficiently fosters self-healing processes. This paper uses randomly generated microstructures of a virtual self-healing dense-graded asphalt mixture and Finite Element (FE) modelling to study the first two aspects. First, the impact of adding capsules of two sizes (1.5 mm and 2.5 mm in diameter) at two different doses (0.5% and 1.0% by total weight of the mix) on the dynamic axial modulus of a mixture was evaluated. Then, two new computational methodologies were proposed to estimate the healing activation potential of the different mixtures. The results show that the capsules caused a small reduction in the dynamic modulus of the mixture, suggesting that they do not compromise this mechanical property. Additionally, over 58% of the capsules could be activated in all cases under the applied load, and the mixture containing capsules with a 1.5 mm diameter added at 1.0% had the highest amount of available healing agent to promote self-healing. The results show that the proposed methods are effective to support some initial design stages of these novel mixtures.

Keywords: Self-Healing; Asphalt Mixtures; Capsules; Finite Elements; Computational Mechanics, Flexible Pavements

1. Introduction

A primary distress in flexible pavements is the appearance and propagation of cracks within the top asphalt layers due to traffic loading, climatic conditions, and binder ageing. Cracking mechanisms include fatigue processes (i.e., fatigue cracking), low-temperature or temperature gradient conditions (i.e., thermal cracking), and hardening oxidation of the asphalt binder (i.e., block cracking) (Roberts et al., 1996). Conventional maintenance and rehabilitation strategies, such as crack sealing, surface replacement, patching, micro-surfacing, chip sealing, in-situ recycling, and full-depth reclamation, among others (ASTM International, 1997; Islam & Tarefder, 2020; Lavin, 2003), are commonly used to repair these distresses, but they increase the maintenance costs and greenhouse gases emissions of the projects (FEHRL, 2008; Tabaković & Schlangen, 2016; Walls & Smith, 1998). This has motivated the assessment of novel solutions to extend the service life of pavements. One initiative consists in enhancing the extrinsic healing properties of the asphalt binder to promote assisted or autonomous crack sealing within the asphalt layers of the pavement (e.g., Ayar et al., 2016; Gallego et al., 2013; Garcia et al., 2016; Liu et al., 2011; Norambuena-Contreras & Garcia, 2016; Yan Li & Zhang, 2021).

Three different techniques proposed during the last 15 years to foster crack-healing in asphalt mixtures include: i) electromagnetic induction, ii) microwave radiation, and iii) addition of encapsulated rejuvenators (i.e., capsules) to the asphalt mixture (Gonzalez-Torre & Norambuena-Contreras, 2020). In the first two cases, electromagnetic induction or microwave radiation is externally applied on the surface of the pavement to increase the temperature of the mixture. This reduces the viscosity of the asphalt binder, promoting the sealing of existing cracks mainly through capillary processes (Ayar et al., 2016; Kargari et al., 2022; Liu et al., 2011). In the third method, capsules with a biopolymeric structure containing a healing agent are added during the fabrication of the mixture. The chemical and rheological properties of the aged asphalt binder near a micro-crack can be partially restored through the softening effects of the released healing agent, promoting the sealing of existing microcracks (Anupam et al., 2022; Garcia et al., 2015; Liang et al., 2021; Su et al., 2013; Xu et al., 2019).

Two main types of capsules have been used in this later technique: i) ‘core-shell’, which consists of a synthetic polymeric shell filled with a healing agent, and ii) ‘polynuclear’ or ‘multi-cavity’, which consists of a biopolymeric structure with multiple cavities (‘egg-box’) filled with a healing agent. In the first case (‘core-shell’), the agent is released when the polymeric shell is broken. In contrast, in the second case, the agent is released from one or more cavities when the polynuclear capsules are deformed or ‘squeezed’ under high-stress concentration conditions (e.g., stresses near the crack tip) or broken at a specific cavity. Typical healing agents used in these capsules are vegetable oils (Al-Mansoori et al., 2017; Garcia et al., 2016; Micaelo et al., 2020, Concha et al., 2024), and waste oils (Al-Mansoori, Norambuena-Contreras, & Garcia, 2018; Norambuena-Contreras et al., 2021, 2022; Yamaç et al., 2021). The size of these capsules varies between 100 and 800 μm for microcapsules (majorly in ‘core-shell’ capsules), and between 1.0 and 7.0 mm for macrocapsules with a polynuclear morphology (Gonzalez-Torre & Norambuena-Contreras, 2020).

The self-healing capacity of the asphalt mixture is expected to increase with the amount of oil released from the capsules. Therefore, a main challenge with this technique is to identify the size of the capsules and the optimum addition dose to maximize the self-healing capacity of the mixture, without compromising its mechanical properties. Previous experimental investigations using macrocapsules with diameters ranging from 2.0 to 7.0 mm, added at doses between 0.1 and 6.0% of the total weight of the asphalt mixture, suggest that while they occasionally reduced the stiffness of the mixture, they had no adverse effects on its resistance to permanent deformation or durability (Norambuena-Contreras et al., 2018; Norambuena-Contreras, Liu, et al., 2019).

Table 1 summarizes the rejuvenator agent, size, dosage, and morphology of macrocapsules –which is the type selected for this study– used in several experimental efforts reported in the literature. Most of these experimental studies have focused on quantifying the healing capacity level of mixtures with capsules under various internal (i.e., mixture types and mixtures with different types and amounts of capsules) or external (i.e., temperature, loading, healing periods, etc.) conditions. Experimental plans include the evaluation of the crack-sealing capacity of these systems in asphalt binders, mastics, mortars or mixtures using a variety of test protocols (Xue et al., 2017; Aguirre et al., 2017; Zhang et al., 2018; Norambuena-Contreras et al., 2018; Xu et al., 2018; Sun et al., 2019; Yamaç et al., 2021; Wang et al., 2022). However, few studies have

evaluated the impact of adding capsules on some critical properties in the early service life of the asphalt mixture (e.g., linear viscoelastic properties or rutting resistance), prior to the initiation of cracking processes (e.g., Micaelo et al., 2020; Concha et al., 2024), or on the self-healing initiation mechanisms. Computational mechanics provides an efficient alternative to conventional experimental approaches for attempting studies in this direction.

Table 1. Typical macrocapsules properties based on published research identified in the literature.

Reference	Healing agent	Size of macrocapsule	Dose (% by the total weight)	Morphology type (-)
(Garcia et al., 2016)	Sunflower oil	2.0-7.1 mm	5%	core-shell
(Kargari et al., 2022)	Palm oil	3.0 mm	0.35-0.7%	polynuclear
(Micaelo et al., 2020)	Sunflower oil	2.8 mm	0.5-1%	polynuclear
(Al-Mansoori et al., 2017)	Sunflower oil	2.9 mm	0.1-0.5%	polynuclear
(Yamaç et al., 2021)	Waste oils	1.5-4.0 mm	0.25-1%	polynuclear
(Norambuena-Contreras, Liu, et al., 2019)	Sunflower oil	2.5 mm	0.5-1%	polynuclear
(Micaelo et al., 2016)	Sunflower oil	4.6-6.8 mm	3-6%	core-shell
(Norambuena-Contreras, Yalcin, et al., 2019)	Sunflower oil	2.5 mm	0.5%	polynuclear
(L. Zhang et al., 2019)	Sunflower oil	2.1-4.6 mm	0.5%	polynuclear
(Norambuena-Contreras et al., 2020)	Bio-oil (BO) from agricultural waste	1.37-2.73 mm	N/A	polynuclear
(Ziari et al., 2023)	Waste sunflower oil and waste engine oil	1.0-2.0 mm	1%	core-shell
(Concha et al. 2024)	Sunflower oil	1.50 mm	0.5%	polynuclear
(Norambuena-Contreras et al. 2024)	Sunflower oil	1.58 mm	0.125-0.5%	polynuclear

The studies by Gilabert et al. (2015), Maiti et al. (2006). Mauludin et al. (2018) Mauludin & Oucif (2018, 2019), and Mauludin & Rabczuk, (2021), among others, have evaluated the mechanisms that initiate self-healing processes on polymers and hydraulic concrete using Finite Elements (FE) and cohesive zones modelling. The objectives of these efforts have been: i) investigate how the properties of core-shell capsules impact self-healing processes; and ii) understand the interaction and fracture mechanisms between the capsules and the matrix in which they are embedded. However, they do not consider the propagation of multiple cracks, the distribution of capsules throughout the matrix, the diverse stress conditions experienced by the

self-healing materials over their service life, and the impact of the presence of the capsules in the mechanical performance of the materials.

Although there are some numerical efforts to assess the natural self-healing capacity of asphalt materials (e.g., Abu Al-Rub et al., 2010; Magnanimo et al., 2012; Pauli, 2014; Hou et al., 2015), few computational works on self-healing asphalt mixtures with capsules were identified in the literature. Inozemtcev et al. (2022) used FE modelling to evaluate the mechanical response of a self-healing Stone Matrix Asphalt (SMA) mixture with one size of 1.3 mm diameter capsules added at a single dose of 1.6% by total volume. The authors evaluated the stress state of the capsules in three-dimensional (3D) mixtures under different loading conditions. Although valuable, this work has several simplifications, including the assumption that the response of the capsules is linear elastic with an arbitrary Young's modulus, and the use of spheres of uniform size to simulate core-shell capsules, aggregate particles and air voids. In short, these considerations can lead to inaccurate mechanical results. Câmara et al. (2023) used Discrete Element Modelling (DEM) at the meso-scale to quantify the influence of different amounts of a released agent on the mechanical properties of the mastic and on the bulk stiffness of a mixture. The work used a 3D geometry with spheres representing both aggregates and the asphalt mastic, and the mechanical properties of the mastic phase was modified as a function of different dosages of the released healing agent (i.e., different healing efficiency scenarios) within the microstructure. In other words, the presence of the capsules and the release of the healing agent were not simulated, as the focus was on the overall mechanical response of a post-healed mixture.

To address existing limitations and further investigate the mechanical response of self-healing asphalt mixtures with capsules, this computational study has two main objectives: i) investigate the impact of the addition of capsules on the dynamic axial modulus of the material ($|E^*|$), and ii) propose a method for an initial quantification of the *activation potential* of the capsules and the *available healing agent*. The *activation potential* is related to the number of capsules that could start to release the healing agent under specific micromechanical stress conditions, while the *available healing agent* refers to the total mass of oil that could be released from the capsules with activation potential and that is available to promote healing processes within the microstructure.

To achieve these goals, the mechanical response of multiple two-dimensional (2D) randomly generated microstructures of an asphalt mixture with polynuclear capsules of two different sizes (1.5 and 2.5 mm in diameter) added at two doses (0.5 and 1.0% by total weight of the mixture), was evaluated using the FE modelling software Abaqus®. It is noteworthy that the selected sizes of the capsules and addition dosages cover most case studies reported in the literature. The geometries of the microstructures were produced using an adaptation of the random Microstructure Generator (MG) code (Castillo et al., 2015).

A key contribution of this computational study is that it offers new insights into how capsules affect a fundamental mechanical property of asphalt mixtures and on their activation mechanisms. Moreover, the computational method is a cost-efficient technique to further explore self-healing mixtures under several conditions (e.g., mechanical loading, different temperatures or ageing states) and to support decision-making processes related to the design of these new materials.

2. Methodology

The computational plan included the following stages (Figure 1):

1. Generation of multiple 2D random models of asphalt mixtures with and without capsules. Four cases were evaluated for the mixtures with capsules: capsules of two different sizes (1.5 and 2.5 mm) added at two different doses (0.5 and 1.0% by total weight of the mixture). The generation method ensures that the resulting 2D microstructures capture the actual 3D response of the mixtures.
2. Virtual dynamic axial modulus ($|E^*|$) of the random microstructures.
3. Application of a monotonic compression test to quantify the *activation potential* of the capsules and the *available healing agent* in the mixture. This computation was performed after considering two different activation micro-mechanisms: i) release of the healing agent due to the application of significant compressive deformation of the capsules, or ii) release of the healing agent due to the fracture of the cavities of the biopolymeric structure of the capsules.

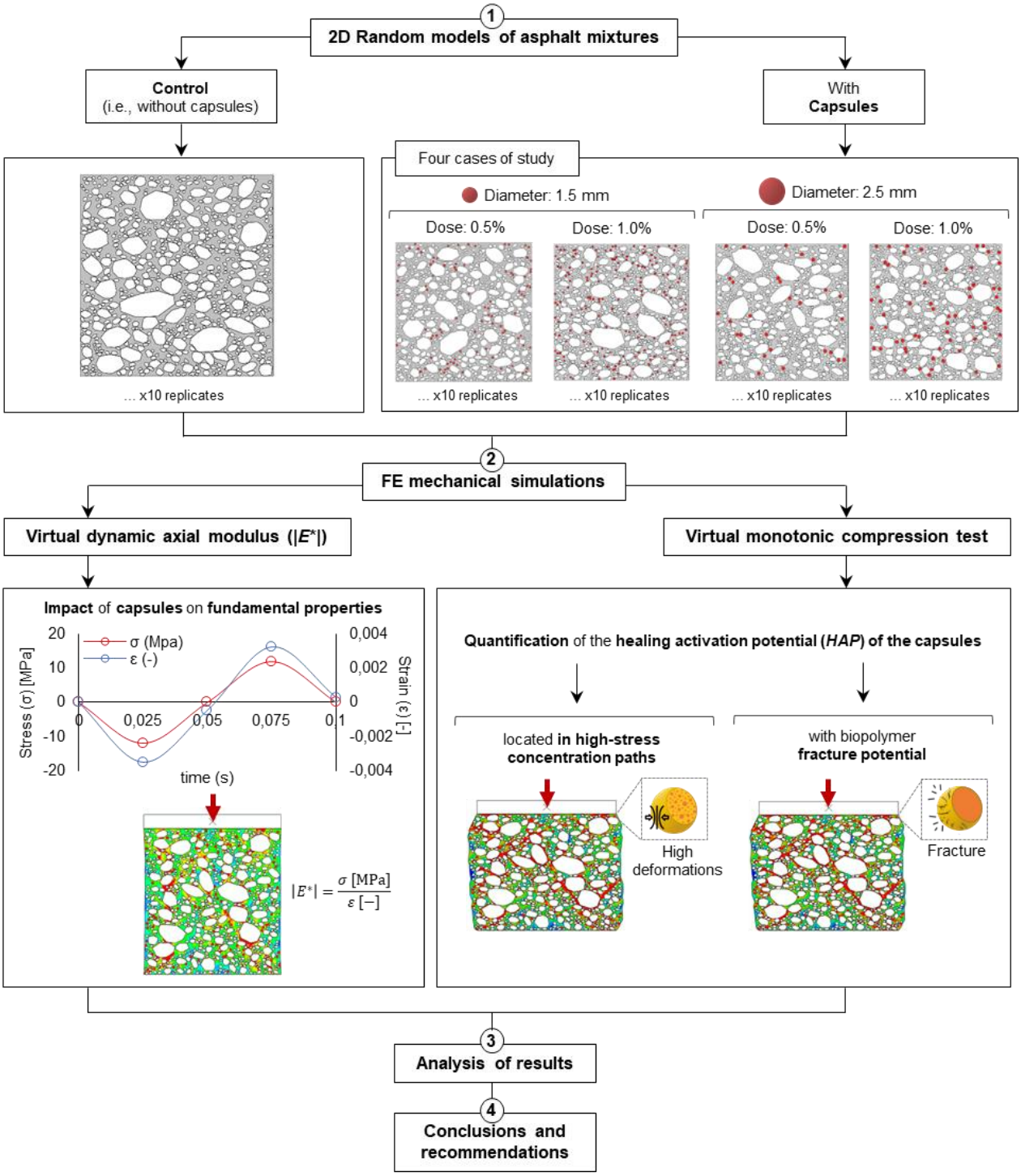

Figure 1. Summary of the computational methodology.

3. Materials

The selected mixture is a standard dense-graded asphalt mixture used as a surface layer, fabricated with sandstone aggregates with a nominal maximum aggregate size of 12.5 mm (Espinosa et al., 2020). The mixture was designed using the Superpave methodology with a penetration 60-70 (1/10 mm) bitumen added at an optimum content of 4.5% by total weight and a target of 7% air voids.

The capsules were polynuclear produced with a biopolymeric structure of calcium alginate and sunflower oil as the healing agent. This selection is based on the literature review, which showed that this is the predominant type of capsules currently used (Table 1). The mechanical properties of the components of the virtual asphalt mixture model and of the capsules are described in the following sections.

4. Computational FE Representative Models

4.1. Geometries

The development of the FE models started with the generation of 2D random microstructures with the properties of the selected asphalt mixture. Data-driven 2D models were preferred over three-dimensional (3D) models due to: i) the reduced computational cost, which permitted to assess several variables (e.g., capsule sizes and doses) and evaluate the impact of the natural heterogeneity of the mixtures by simulating multiple randomly produced replicates per case, something that is difficult to achieve in 3D models, and ii) the possibility to account for more realistic geometries to represent the aggregate particles and the capsules as those used in previous works (Mauludin et al., 2018; Mauludin & Rabczuk, 2021; Inozemtcev et al., 2022; Câmara et al., 2023).

A tailored method was designed to generate these 2D microstructures that capture the 3D response of the asphalt mixture, utilising principles similar to those proposed in previous works (Karki, 2010; Manrique-Sanchez et al., 2022). The microstructures have three phases: i) coarse aggregates (i.e., aggregates larger than 1.18 mm), ii) asphalt mortar (i.e., mix of the asphalt binder with the fine portions of aggregates –which correspond to aggregates smaller than 1.18 mm– and air voids), and iii) capsules. These components are illustrated in one typical microstructure in Figure 2, where capsules are coloured in red, aggregate particles in white, and the grey ‘background’ corresponds to the asphalt mortar. The overall size of the microstructures was 100 mm by 100 mm, following existing recommendations in the literature to ensure representative

volume elements (RVE) (Kim et al., 2005, Caro et al., 2018; Castillo et al., 2015, 2017, 2018). The control microstructures are similar to these geometries, but they do not contain capsules. All the microstructures generated for the study are random and unique.

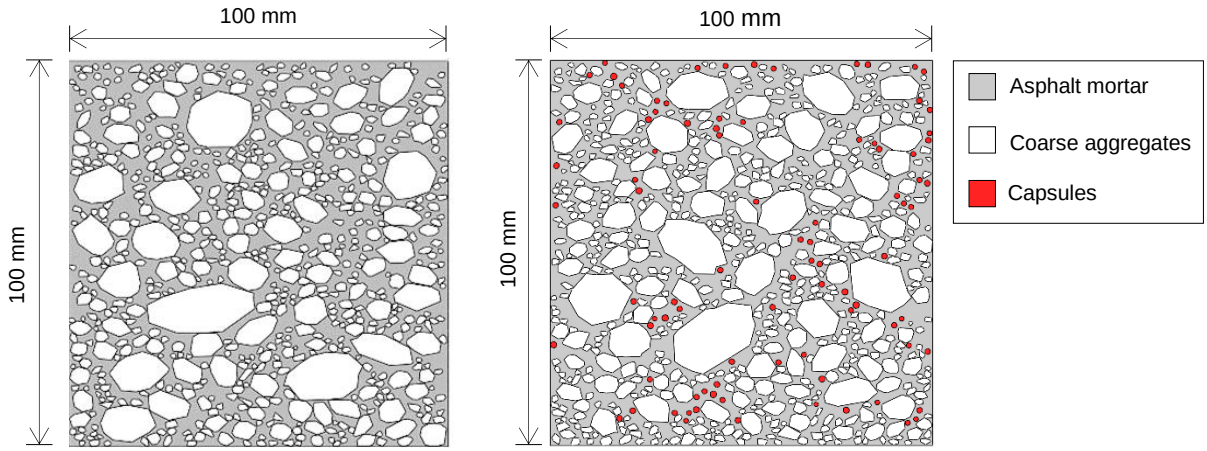

Figure 2. Examples of the randomly generated virtual microstructures: (a) asphalt mixture without capsules (i.e., control), and (b) asphalt mixtures with capsules.

The 2D microstructures with and without capsules were generated after adapting the random Microstructure Generator (MG) Matlab® code developed by Castillo et al. (2015). The random generation of the coarse aggregates in the data-driven MG requires three input parameters: i) the gradation of the mixture, ii) the morphological properties of the individual aggregates, and iii) the total aggregate fraction area of the mixture, defined as the proportion of area of coarse aggregates to the area of the specimen. The morphological properties of the aggregates are characterized through the Angularity Index (AI) and the Form Index (FI) of the individual particles (Castillo et al., 2018). Target values of AI and FI of 0.076 and 2.460 were selected after comparing the resulting aggregate polygons with those of real images of self-healing asphalt mixtures.

The area fraction of the aggregates within the mixture was determined through image analysis using ImageJ software on X-ray CT in 2D images of a self-healing asphalt mixture (Norambuena-Contreras et al., 2018; Norambuena-Contreras et al., 2019). The results showed that nearly 50% of the total image area corresponded to the aggregate phase. Using this observation and the methodology proposed by Manrique-Sanchez et al. (2022), a calibration process was performed to determine the fraction phase of aggregates in the 2D models that resulted in a FE-quantified dynamic axial modulus ($|E^*|$) comparable to experimental data of $|E^*|$ in actual 3D

mixtures. This ensures that the models capture the mechanical response of actual asphalt mixtures, while avoiding the high computational costs of 3D models. The selected aggregate fraction area in the microstructures was 50%. For illustrative purposes, Figure 3 compares the mixture composition in a CT scan image of a mixture with capsules (Norambuena-Contreras et al. 2018; 2019) with one of the randomly generated microstructures used for the FE simulations.

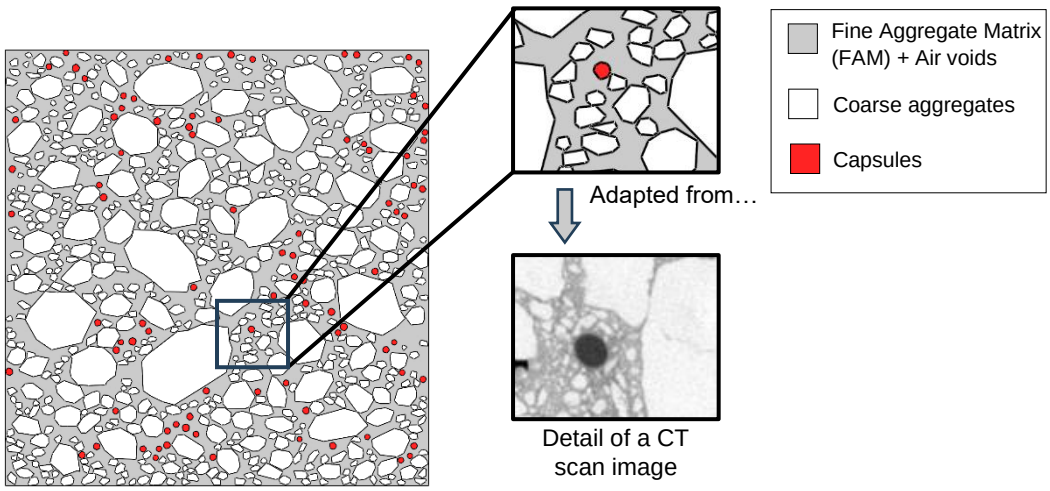

Figure 3. Comparison of the composition of the mixture between a real self-healing asphalt mixture containing polynuclear capsules (CT scan image) and one of the 2D random microstructures used in the FE models.

The diameter of the individual polygons representing the capsules followed a probability density function (*pdf*) that accounts for size variations resulting from the capsule fabrication process. These variations are caused by differences in the settling time of the emulsion droplets into the hardening solution, which initiates biopolymer cross-linking. The *pdf* was determined using the experimental results published by Norambuena-Contreras et al. (2021). The range of sizes, the mean value (λ) and the standard deviation (ξ) of the *pdf*s were: i) [1.20 mm, 1.86mm], λ = 0.41andd ξ = 0.08, for the 1.5 mm capsules, and ii) [2.20 mm, 2.83mm], λ = 0.92andd ξ = 0.06, for the 2.5 mm.

The fraction area of the capsules at each dose (0.5 and 1.0% by total weight) in the models was assumed equivalent to the volumetric fraction of the capsules in the mixture evaluated by Norambuena-Contreras, et al. (2019). The dimension and bulk density of the specimen, as well as the diameter, dose, and density of the capsules, were used to compute these values. The resulting fractions of the capsules for the doses of 0.5% and 1.0% were 1.32% and 2.64% of the total area,

respectively. Since the addition of capsules is by weight of the mixture, the actual number of added capsules was different in all cases. The typical number of 1.5 mm capsules added at a dose of 0.5% and 1.0% were 90 and 182, respectively, while the number of 2.5 mm capsules added at the same doses was 30 and 61, respectively.

Once the individual sets of coarse aggregates and capsules were generated, they were randomly located in a predetermined geometrical space. A new function to locate aggregates and capsules was included in the MG program to guarantee that the capsules were uniformly distributed within the asphalt mixture.

4.2. Cases of study

A total of five cases (i.e., two different sizes of the capsules added at two different doses, and a control case of microstructure with no capsules) were evaluated. Examples of one microstructure from each case are presented in Figure 4.

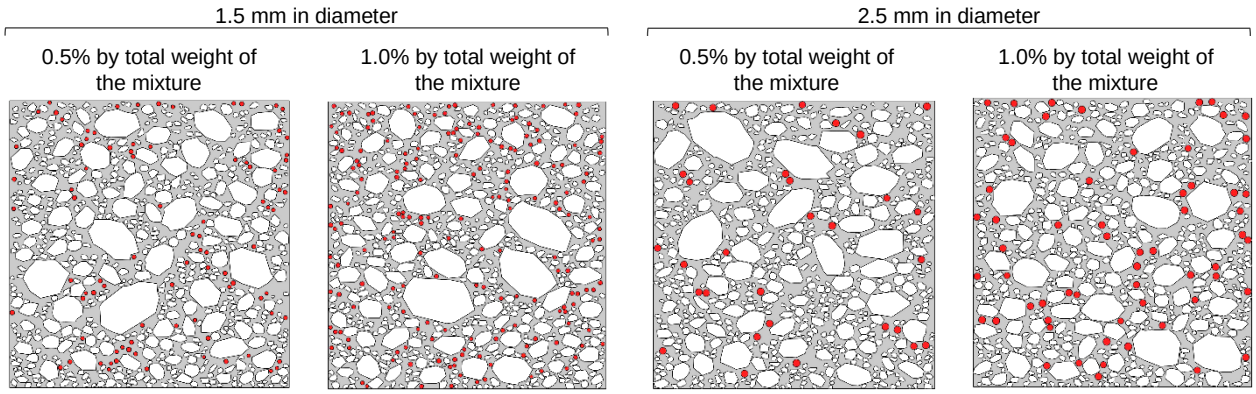

Figure 4. One computational replicate for the mixtures with capsules.

To capture the natural heterogeneity of the mixture, 10 different random microstructures or 'virtual replicates' per case of study were generated and imported into FE. Figure 5 presents five out of the 10 virtual replicates for the case of 2.5 mm capsules added at 1.0% by weight. The differences in the size and location of the coarse aggregate particles and capsules between the replicates are easily identified. In total, 50 computational microstructures were modelled, 40 for the cases of study with capsules, and 10 for the control microstructures.

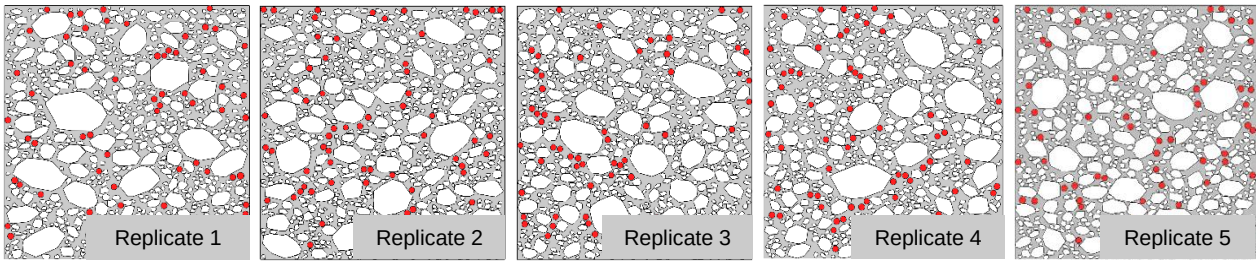

Figure 5. Five virtual replicates for the case of 2.5 mm capsules added at 1.0% by the total weight of the mixture.

4.3. Constitutive Response of the Materials of the Model

In the FE models, the aggregates were assumed to behave as a linear elastic material with a modulus of 10,000 MPa and a Poisson's ratio of 0.16 (Castillo et al., 2018), which is within the range of Young's modulus values for sandstone rocks (Weijermars, 1997). The asphalt mortar was modelled as a homogenous phase with a bulk specific gravity of 2.1, based on a previous study developed by Romero (2019), with a linear viscoelastic response presented by the Prony series parameters of the relaxation modulus of the material at 25 °C. These parameters were obtained by transforming the dynamic axial modulus (|*E**|) data of an asphalt mortar from the frequency to the time domain. The Prony series of the shear relaxation modulus of a material can be expressed as:

$$g(t) = 1 - \sum_{i=1}^{n} g_i(1 - e^{-t/\rho_i}) \quad (1)$$

where $g(t)$ is the normalized shear relaxation modulus of the material, which is defined as the relaxation modulus or $G(t)$ normalized with respect to the instantaneous shear modulus (G_0), t is the time, g_i is the ith normalized Prony series parameter (i.e., the ratio between the original Prony series parameter G_i and the instantaneous shear modulus G_0 (i.e., $g_i = G_i/G_0$)), and ρ_i is the ith relaxation time (Fabrizio & Morro, 1987). Table 2 presents the parameters of the original Prony series used as a base, including the axial instantaneous modulus (E_0(t)).

The mechanical response of the capsules was also linear viscoelastic. The capsules were assumed to be a continuum phase with properties representing the bulk response of this composite material. Since experimental information of the viscoelastic response of these capsules is not currently available, FE simulations were performed to estimate the equivalent linear viscoelastic properties of the capsules, after conducting a virtual relaxation modulus test on models representing the capsules. The viscoelastic properties of the calcium-alginate biopolymer and the

sunflower oil at 25 °C were obtained from the literature (Fabrizio & Morro, 1987; Xiang et al., 2016). Table 3 presents the resulting Prony series parameters that represent the viscoelastic response of the two sizes of capsules.

Table 2. Prony series parameters of the asphalt mortar at a temperature of 25°C (Romero & Caro, 2019).

i	ρ_i (s)	G_i (Pa)
1	0.000001	8.05×10^5
2	0.00001	7.38×10^5
3	0.0001	1.94×10^6
4	0.001	3.43×10^7
5	0.01	4.70×10^8
6	0.1	2.54×10^8
7	1.0	5.69×10^7
8	10	4.04×10^7
9	100	1.51×10^7
10	1,000	6.26×10^6
11	10,000	8.11×10^6
	E_0 (MPa)	1,200

Table 3. Prony series parameters of the capsules at a temperature of 25°C.

i	ρ_i (s)	Diameter of the capsules	
		1.5 mm	2.5 mm
		G_i (Pa)	G_i (Pa)
1	0.0003	5.58×10^7	4.74×10^7
2	0.001	4.70×10^7	3.99×10^7
3	0.003	3.96×10^7	3.36×10^7
4	0.01	3.29×10^7	2.79×10^7
5	0.03	2.81×10^7	2.39×10^7
6	0.1	2.37×10^7	2.01×10^7
7	0.03	2.81×10^7	2.39×10^7
8	0.4	1.96×10^7	1.66×10^7
9	1.0	1.68×10^7	1.43×10^7
10	3.2	1.41×10^7	1.20×10^7
11	9.4	1.20×10^7	1.02×10^7
12	10	1.19×10^7	1.01×10^7
13	93	8.54×10^6	7.26×10^6
14	929	6.06×10^6	5.15×10^6
15	9,303	4.30×10^6	3.66×10^6
16	10,000	4.26×10^6	3.62×10^6
	E_0 (MPa)	850	1,000

5. Mechanical Simulations

After the geometry of microstructures were imported into FE, the three phases (i.e., aggregates, capsules, and mortar) were meshed. Based on a sensitivity analysis, the average size of the

297 elements was 1 mm using triangular elements type CPE3 in Abaqus®. The virtual microstructures
298 were subjected to two different mechanical tests, as described next.

299 ***5.1. Dynamic Axial Modulus Test***

300 In the dynamic axial modulus test, the microstructures were subjected to a cyclic loading of 1,190
301 N at a frequency of 10 Hz and at a temperature of 25 °C. Figure 6(a) illustrates the Mises stress
302 distribution (*S*) (Karakaş et al., 2014) of a virtual specimen during the first cycle of the load applied
303 in the FE model. The applied force amplitude is within typical ranges for this test specified in
304 existing standards (e.g., AASHTO T342-11). Meanwhile, Figure 6(b) shows the load signal and
305 its corresponding axial deformation response, which allows the determination of the dynamic axial
306 modulus, $|E^*|$ (i.e., the ratio between the amplitude of the applied load signal, σ_0, and the axial
307 deformation signal, ε_0), and the phase angle, ϕ (i.e. the lag between the stress and strain signal),
308 for the virtual specimens.

309 ***5.2. Monotonic Compression Test***

310 A new methodology is proposed to estimate the *activation potential* and *available healing agent*
311 to initiate healing processes in these mixtures. To illustrate this methodology, a monotonic
312 compression test was performed on the same set of microstructures. These tests have been used in
313 experimental studies to activate the capsules of fractured asphalt mixture specimens to promote
314 healing processes, under the assumption that the applied load simulates the pass of heavy traffic
315 on the surface of the pavement structure (Al-Mansoori, Norambuena-Contreras, Micaelo, et al.,
316 2018; Concha et al., 2024; Kargari et al., 2022; Norambuena-Contreras et al., 2018; Norambuena-
317 Contreras, Yalcin, et al., 2019).

318 The microstructures were subjected to a controlled compressive displacement of 7.5 mm
319 applied progressively for 15 minutes (i.e., loading rate of 0.5 mm/min). The objective was to
320 identify individual capsules that could release their healing agent and the corresponding amount
321 of available oil to initiate healing processes using two approaches related to different activation
322 micro-mechanisms (Concha et al., 2023): i) identification of capsules located in high-stress
323 concentration paths (i.e., activation by high compressive deformation of 'squeezing' mechanisms),
324 and ii) identification of capsules that could get fractured (i.e., activation by fracture of the
325 biopolymer structure of the capsule).

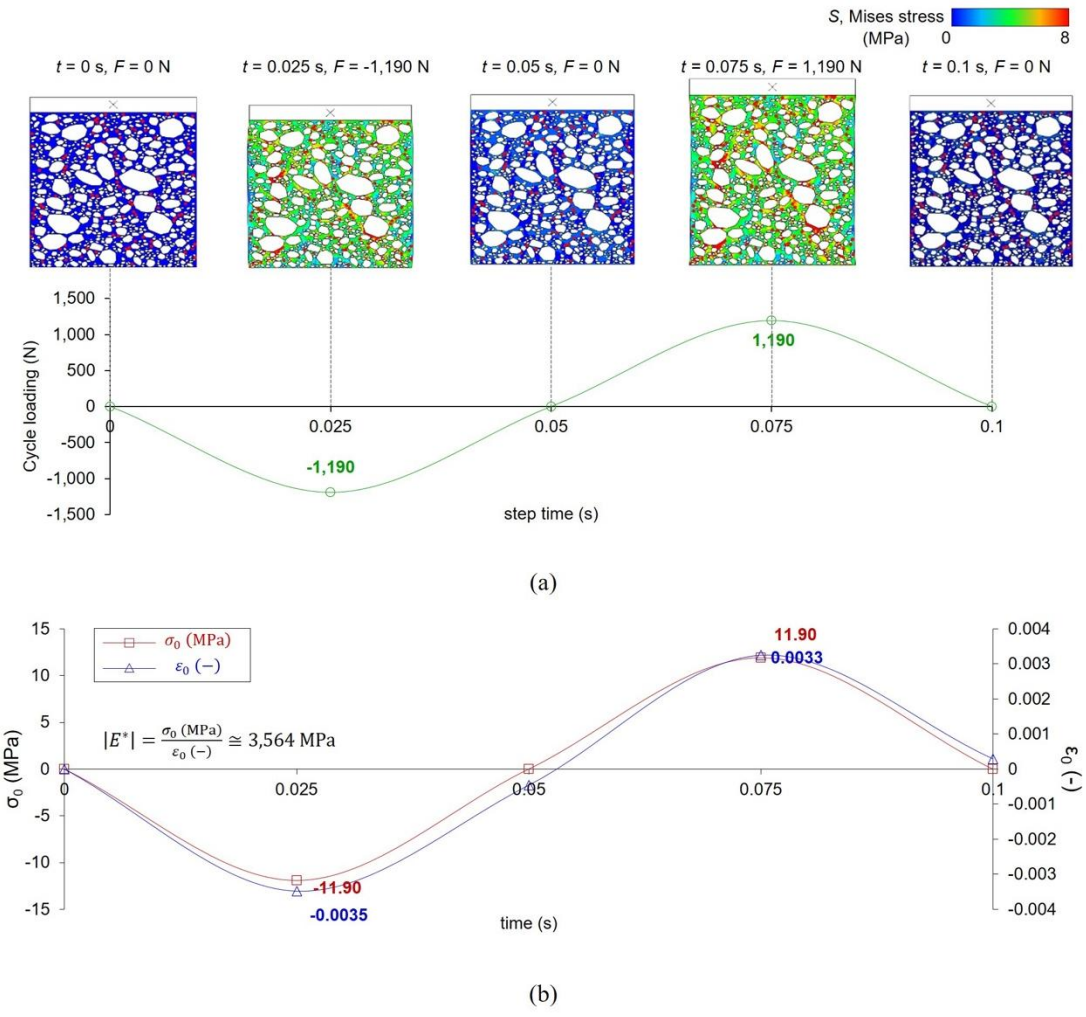

Figure 6. Dynamic axial modulus virtual test: (a) applied load, F, (deformation scale factor = 15), (b) applied stress ($\sigma(t)$) and deformation response ($\varepsilon(t)$). Specimen with 1.5 mm capsules added at 0.5% by total weight.

In both cases, it was assumed that all capsules are intact at the beginning of the mechanical test, which is a fair simplification, as existing X-ray computed tomography (CT) analysis on self-healing mixtures have shown that only a minor percentage of capsules (less than 6.0% of the total capsules) could be broken or damaged during the compaction of the mixtures (Micaelo et al., 2016, Norambuena-Contreras et al., 2018; Liu, et al., 2019; Zhang et al., 2019).

5.2.1. First approach: capsules located on high-stress concentration paths

The first approach is based on the premise that polynuclear capsules located within high-stress concentration paths are subjected to high deformation conditions (i.e., the capsules are 'squeezed') and, consequently, could start to release the healing agent. Since the appearance of micro-cracks

in a mixture is also expected to occur within these same paths, the released agent will facilitate the healing of surrounding micro-cracks.

Figure 7 illustrates the axial deformation and Mises stress condition during the monotonic compressive test of a replicate of a mixture with 1.5 mm in diameter capsules added at 0.5% by total weight. The image processing program ImageJ was used to quantify the capsules located in high-stress concentration paths (i.e., capsules with *activation potential*) at the end of the monotonic test. Next, an arbitrary threshold stress value of 12.5 MPa was selected to identify capsules located within high-stress paths. This stress level does not represent a condition related with crack initiation in the mortar, but rather a condition useful to identify high-stress concentration paths within this phase. The result is a segmented image like the one presented in Figure 8, that shows the zones of the capsules with stress values equal to or larger than the threshold in black. These capsules could be deformed or 'activated' if sufficient stress concentration levels are developed within the specimen. Figure 9 shows the resulting image analysis for one replicate of each case of study, where the capsules located within high-stress paths (i.e., red capsules with internal black areas) are easily identified.

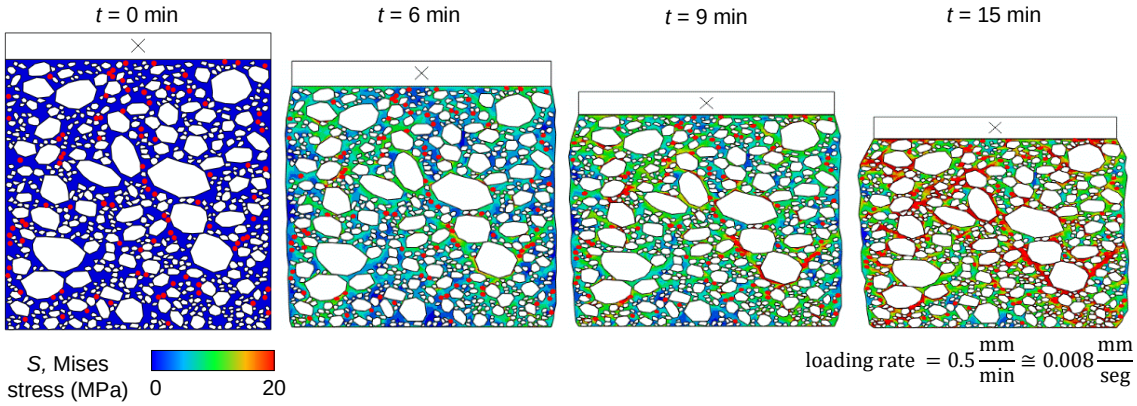

Figure 7. Vertical deformation (scale factor=2.0) and Mises stress (*S*) during the compressive monotonic.

The capsules with *activation potential* in the dark grey paths, like those in Figure 9, were counted and used to compute the *healing activation potential* (HAP_{paths}), defined as the ratio of the number of capsules within high stress paths $C_{activation\ through\ deformation}$, and the total number of capsules in the mixture, C_{total}:

$$HAP_{paths} = \frac{C_{activation\ through\ deformation}}{C_{total}} \quad (2)$$

The higher the HAP_{paths}, the higher the possibility for the healing agent to be released and to initiate healing processes under this loading condition.

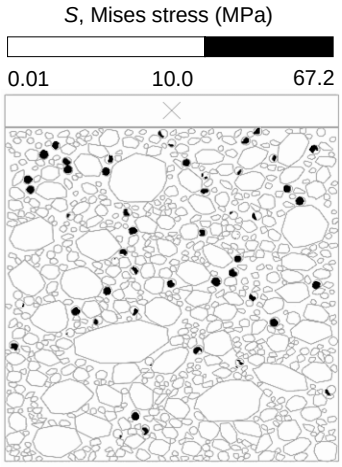

Figure 8. ImageJ processed image showing the capsules with *activation potential*.

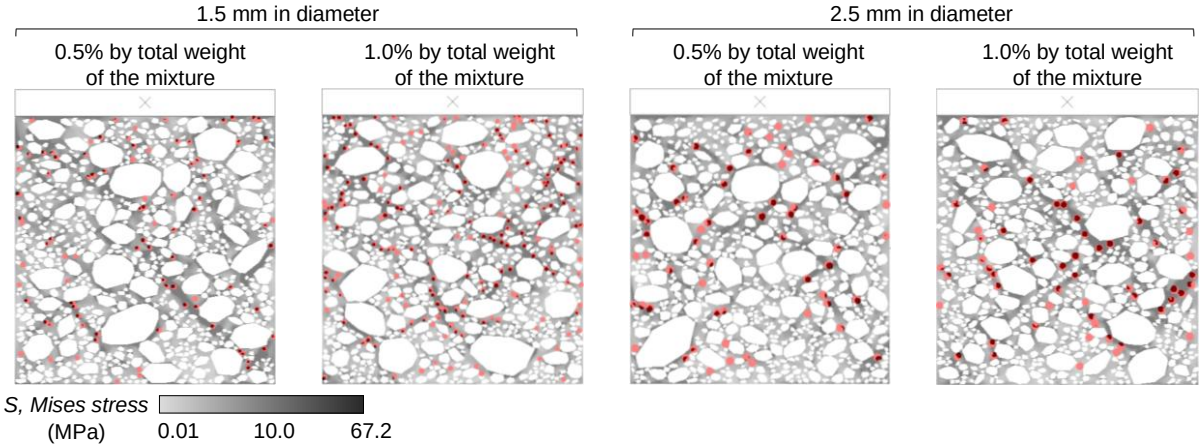

Figure 9. Mises stress paths in one replicate per case at the end of the monotonic test. Red capsules with internal black areas are within high concentration stress paths.

5.2.2. Second approach: capsules with fracture potential

The second approach considers the potential fracture of the biopolymer cavities of the capsules. It is based in the identification of the zones in the capsules with tensile stress levels larger than 33.6 MPa, which, according to Rhim (2004), corresponds to the tensile strength of the biopolymer used to fabricate the capsules. This approach assumes that Mode I is the predominant mode of fracture of the biopolymer, although this is an initial estimation of the actual fracture modes in these materials (Manrique-Sanchez et al., 2018).

The average maximum tensile stress (σ_{t-max}) of each capsule was obtained at different times during the monotonic test. The estimation of σ_{t-max} during the progression of the test was done using a Mohr's circle analysis based on the cartesian normal stresses (σ_x, σ_y) and shear stress (τ_{xy}) values obtained at each element of the capsules:

$$\sigma_{t-max} = \frac{\sigma_x+\sigma_y}{2} + \sqrt{\left(\frac{\sigma_x+\sigma_y}{2}\right)^2 + (\tau_{xy})^2} \quad (3)$$

Then, a MATLAB code was developed and used to identify the capsules with σ_{t-max} values exceeding the tensile strength of the biopolymer across their area. These capsules have a high probability of fracture and activation.

Figure 10 shows the evolution of the internal tensile stress of a capsule and the zones where the tensile strength threshold is attained with time (i.e., black zones). A capsule is considered to have *activation potential* if at least 30% of its total area reaches the tensile strength of the biopolymer. This arbitrary criterion considers that the biopolymer should get fractured in multiple locations to release enough liquid agent to initiate healing. The *healing activation potential* ($HAP_{fracture}$) was computed as the ratio between the number of capsules with fracture *activation potential*, $C_{activation\ through\ fracture}$, and the total number of capsules added to the mixture, C_{total}:

$$HAP_{fracture} = \frac{C_{activation\ through\ fracture}}{C_{total}} \quad (4)$$

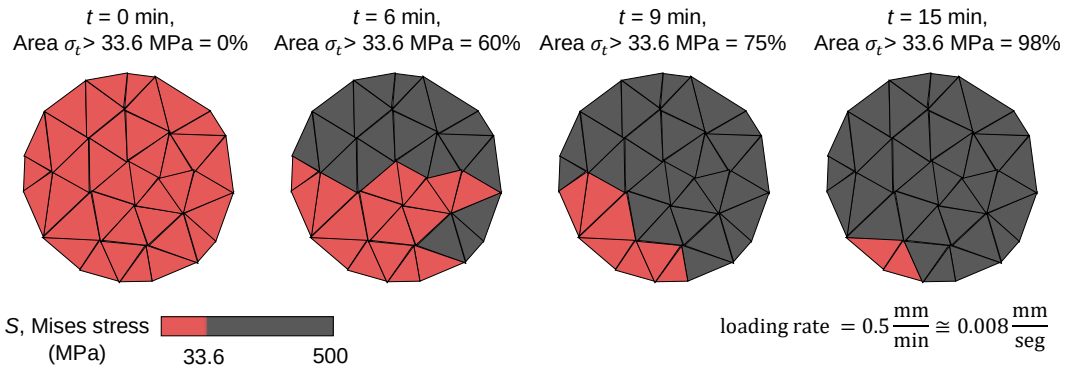

Figure 10. Tensile stress level (σ_t) of a sample of one 1.5 mm capsules during the compressive monotonic load (deformation scale factor = 0).

5.2.3. Available healing agent

Although the previous indices provide information on the maximum theoretical number of capsules that could initiate the release of the healing agent, different mixtures could have similar *HAP* indices but still result in different healing levels. To complement this information, the *available healing agent* was also computed for each method. This parameter is defined as the mass of oil that could be released from capsules with activation potential. It is not realistic to assume that all the oil within the capsules with activation potential will be released. Thus, three different values of *available healing agent* were computed after assuming that the average mass of oil released from the capsules is 100% (maximum theoretical value), 80% and 60%. In a recent study by Concha et al. (2024), the relative mass of biopolymer and healing agent in capsules with different size fabricated with calcium alginate and sunflower oil was reported. Table 4 presents these values. The *available healing agent* was calculated by multiplying the total amount of capsules with activation potential obtained from each method with the maximum mass of oil available per capsule (Table 4) and the three percentages of released agent (i.e., 100, 80 and 60%).

Table 4. Parameters to compute the available healing agent (based on data from Concha et al., 2024).

Cases of study	***Proportion of healing agent available in one capsule (%)***	***Mass of one capsule (g)***
1.5 mm	83%	0.0023
2.5 mm	95%	0.0038

6. Results and Discussion

6.1. Axial Linear Viscoelastic Properties

Figure 11 presents the average results of the dynamic axial modulus, $|E^*|$, with error bars representing to ± one standard deviation from the 10 random replicates. A drop in the magnitude of $|E^*|$ in the mixtures with capsules could be expected due to the differences in density between the asphalt mortar and the capsules. However, data in this figure show no notorious differences in the magnitude of $|E^*|$ of the mixtures with and without capsules. For the cases with 2.5 mm capsules, for example, the drop in the average modulus with respect to the control mixture was less than 1.0%. The highest reduction was 3.0% and it occurred for the case with 1.5 mm capsules added at 1.0% by total weight.

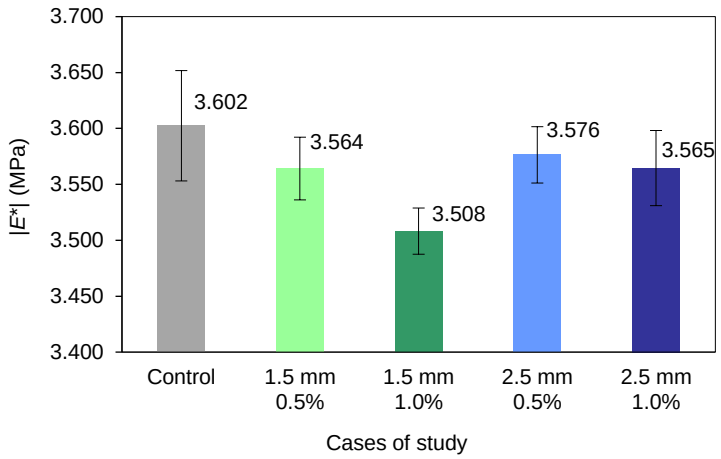

Figure 11. Dynamic axial modulus (|*E**|) results. Notice that the vertical axis starts at 3,400 MPa. Note that the reduction in modulus is small (between 1.0 and 3.0%).

One-Way Analysis of Variance (ANOVA) tests at a significance level of $\alpha = 0.05$ showed that the only case that did not have significant differences in |*E**| with respect to the control specimens was the mixture with 2.5 mm capsules at the lower dose of 0.5%. Despite these statistical differences, the reduction in the modulus was less than 3.0% in all cases. This suggests that the addition of capsules does not impact the stiffness of the mixtures and, therefore, that it is unlikely that the rutting susceptibility of the self-healing mixture could be compromised during the initial service years.

The numerical results were qualitatively compared against existing experimental data of the stiffness of self-healing asphalt mixtures. Norambuena-Contreras et al. (2018) and Al-Mansoori et al. (2017) computed the flexural stiffness modulus of self-healing mixtures (S_m) using the Indirect Tensile Stiffness tests on cylindrical specimens, while Micaelo et al. (2020) computed the dynamic axial modulus of the mixture (|*E**|) using the configuration of the Four-point Bending test (4PBT). In the case of asphalt mortars, Viana-Sepulveda et al. (2023) quantified the dynamic shear modulus (|*G**|) of short-term aged asphalt mortars with 1.5 mm diameter capsules added at a dose of 0.5% by total weight. Figure 12 presents the experimental and numerical results. To ensure a proper comparison, cases with similar sizes and doses of capsules as those used in this study were selected from each study.

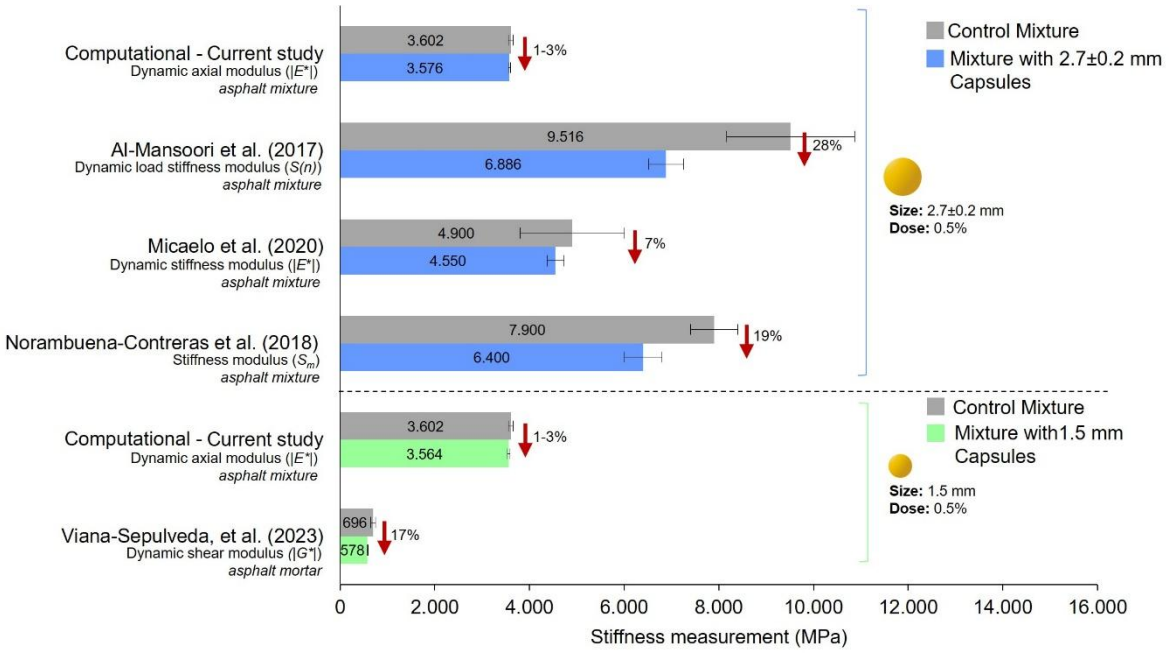

Figure 12. Preliminary validation of the numerical results of $|E^*|$ with experimental results reported in the literature.

These data show that the addition of capsules caused a reduction in the mean experimental stiffness of the asphalt materials that varied between 7 and 28%. However, due to high variability among replicates, the actual differences in these properties with respect to the control materials might not be significant in some of these works (e.g., Viana-Sepulveda et al. 2023). Overall, these experimental results provide a preliminary experimental validation of the numerical outcomes herein obtained, indicating that the randomly produced 2D models provide sound results.

In terms of the phase angle, the resulting values of ϕ were: 9.42° ± 0.82° for the mixtures with no capsules, and 9.49° ± 0.18 and 9.95° ± 0.58° for the mixtures with 1.5 mm capsules added at 0.5 and 1.0%, respectively, and 9.47° ± 0.33° and 9.6° ± 0.3° for the mixtures with 2.5 mm capsules added at 0.5 and 1.0%, respectively. These values are within typical ranges reported in the literature for hot dense-graded mixtures tested at 25 °C and 10 Hz (Biligiri et al., 2010; Rahman & Tarefder, 2018; Hussain et al., 2021). There is an average difference of 2.0% between the mean value of ϕ for all the cases with capsules and the control case, but one-way ANOVA tests show that these differences were not significant (p-value of 0.68). This confirms that the capsules do not compromise the linear viscoelastic properties of the mixture.

It should be noted that the modulus of the mixtures was estimated using cyclic compressive-tensile loading simulations, but that the evaluation of the mechanical properties of these mixtures can be complemented using other loading conditions (Cheng et al., 2021 and 2022).

6.2. Activation Potential of the Capsules

Table 5 shows the Healing Activation Potential (*HAP*) indices and the number of capsules with activation potential obtained from the two methods evaluated (i.e., *paths* and *fracture* at the end of the test).

Table 5. Results of the *HAP* indices and number of capsules activated per case of study.

Cases of study	HAP_{paths}	*Number of capsules with activation potential-paths*	$HAP_{fracture}$	*Number of capsules with activation potential -fracture**
1.5 mm - 0.5%	71% ± 5%	64 ± 4	76% ± 4%	68 ± 4
1.5 mm - 1.0%	74% ± 4%	134 ± 7	75% ± 3%	137 ± 7
2.5 mm - 0.5%	86% ± 5%	26 ± 2	58% ± 10%	17 ± 3
2.5 mm - 1.0%	83% ± 5%	51 ± 3	61% ± 6%	37 ± 4

** Values at the end of the monotonic compression test.*

The *HAP* results ranged between 58 and 86%, indicating that a high proportion of the total capsules in the mixtures could be activated. One-way ANOVA tests at a significance level of $\alpha = 0.05$ were performed for the mean values of HAP_{paths} and $HAP_{fracture}$ among mixtures. The results show that the variation of the addition dose at the same size of capsules (1.5 mm and 2.5 mm in diameter) does not generate significant differences in any of the *HAP* indices, while significant differences were found with a change in the size of the capsule. This suggests that the capsule size is more critical than the addition dose in determining the percentage of capsules with activation potential in the mixture. It is noteworthy that the results of the HAP_{paths} and $HAP_{fracture}$ in this table are not directly comparable, since they are based on different activation micro-mechanisms. While HAP_{paths} counts capsules located within high-stress concentration paths (i.e., potential micro-cracks), $HAP_{fracture}$ counts capsules that could get fractured under Mode I conditions. This explains why the magnitude of *Healing Activation Potential* indexes are smaller for $HAP_{fracture}$ (from 58% to 76%) as compared to HAP_{paths} (from 71% to 83%), as it is more probable that a capsule would be located within a high-stress path during the compression test than to reaching a specific internal stress value.

In terms of the number of capsules with activation potential, data in Table 5 show that, on average, the number of capsules that could be activated through both methods ranged from 26 to

134 in the case of the capsules located in high stress concentration paths, and from 17 to 137 in the case of the capsules with fracture potential at the end of the monotonic test. In the case of the fracture activation micro-mechanism, the number of capsules with activation potential increased with the progression of the test, as observed in Figure 13. This figure shows that the mixture with 1.5 mm capsules added at 0.5% had the highest activation speed during the test (i.e., highest slopes), while the mixture with 2.5 mm capsules added at the same dose of 0.5% had the slowest activation speed.

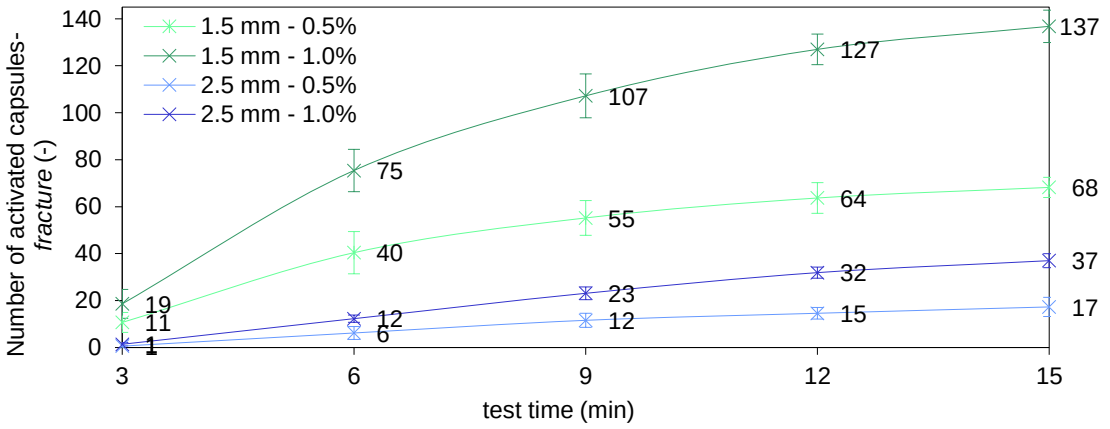

Figure 13. Number of capsules with activation potential due to fracture over the progression of the test.

The resulting coefficient of variation (COV) among replicates for the number of capsules with activation potential in Table 5 ranged between 5.0 and 17.0%, which reflects that the heterogeneity of the microstructure of the mixtures (i.e., spatial location of aggregates and capsules) is not negligible in determining how many capsules could be activated.

The results also show that when the dose of capsule addition doubles, the number of capsules that could be activated –and not only the total amount of added capsules– increases in nearly the same proportion. This has a direct impact on the effective available oil or *available healing agent* that could be released from the capsules. The relevance of this parameter is that it represents the actual amount of effective oil within the self-healing mixtures to start healing processes. The best-case scenario corresponds to a mixture with a high number of capsules with activation potential (i.e., the higher this value, the higher the probability that a capsule will activate near a microcrack), in conjunction with a high amount of available healing agent.

Figure 14 compares the number of capsules with activation potential and the amount of available oil through both methods (*paths* and *fracture*) for the different cases. Recalling, the *available healing agent* was computed after assuming that the capsules could release, on average, 100, 80, and 60% of the encapsulated agent obtained. Notice that the first case is a maximum theoretical value, as it represents the total mass of oil available if all capsules with activation potential would release their entire healing agent. One-way ANOVA tests show that the number of capsules with activation potential and the corresponding amount of available healing agent, significantly differ depending on the capsule size and addition dose. The maximum *p*-value when comparing the impact of the capsule size was 0.02, while for the capsule dose this value was 0.002. These results show that both, capsule size and addition dose, are important in determining the self-healing potential of the mixtures.

An interesting observation is that the results of the available healing agent are similar through both activation mechanisms for the mixtures with 1.5 capsules, with differences of less than 7.0% among equivalent cases, while there are relevant changes in this parameter for the mixtures with 2.5 mm, with differences of up to 37.0%. This suggests that bigger capsules are more sensitive to the type of activation mechanism.

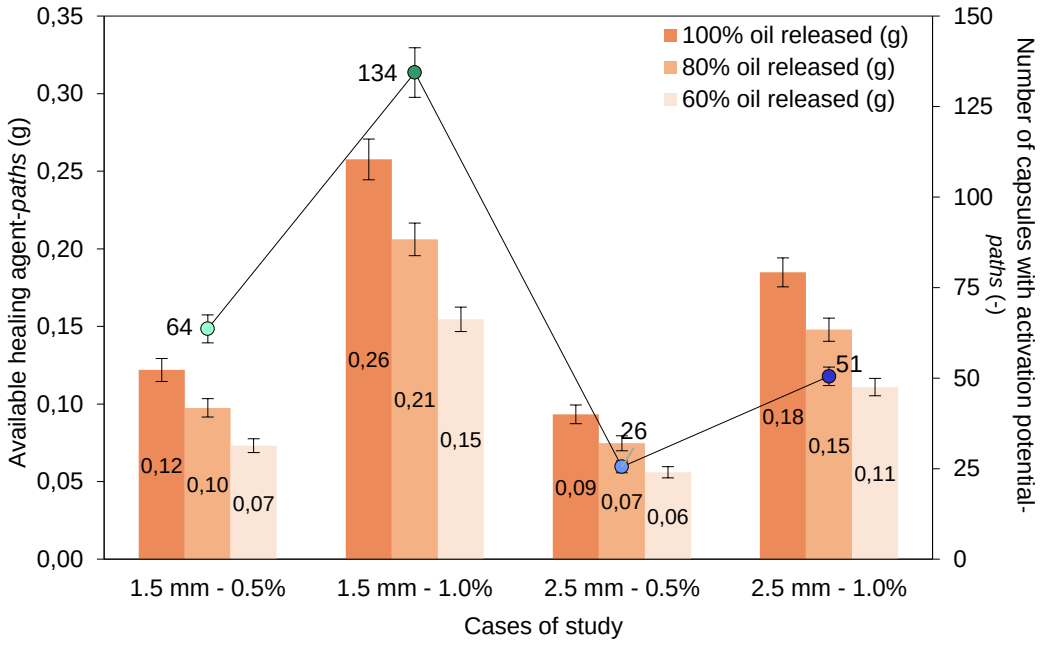

(a)

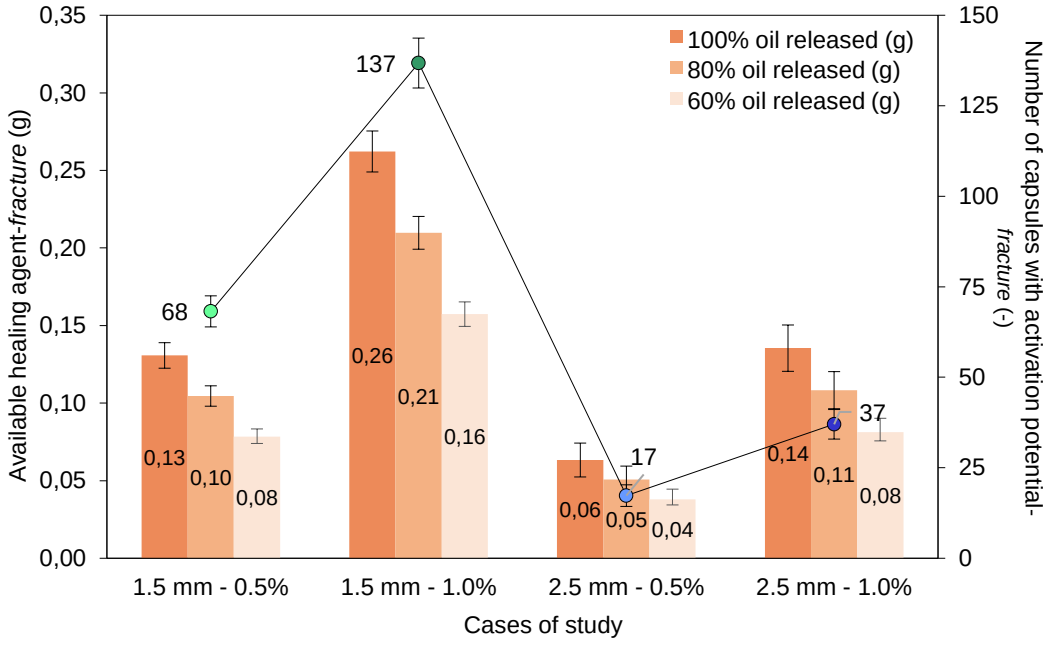

(b)

Figure 14. Number of capsules with activation potential and amount of available healing agent a function of the activation method: (a) high deformation of the capsules (-*paths*), and (b) fracture of the capsules (-*fracture*).

The results in this figure also highlight that the same capsule dose does not necessarily lead to the same amount of available released oil, as might have been expected. For instance, at the same addition dose of 0.5% (i.e., same total mass of added capsules to the mixture), the results in Figure 14(b) show that the available mass of healing agent is between 0.08 and 0.13 g for the mixture with 1.5 mm capsules, while this value is only 0.04 and 0.06 g for the mixtures with 2.5 mm capsules (i.e., 50% reduction). Notably, smaller capsules have a higher number of potential activation points and a higher amount of available healing agent. This result shows that, even though the mass proportion of oil in comparison with the biopolymer mass in the 1.5 mm diameter capsules is lower than that in the 2.5 mm diameter capsules (83% vs. 95%, as shown in Table 4), this is offset by the increased number of activation points within the mixture. In fact, data in this figure indicate that the mixture containing 1.5 mm capsules at a 1.0% dosage is particularly promising, as it exhibits the highest capsule activation potential (134-137 of capsules with activation potential, on average, for -*paths* and -*fracture*, respectively), resulting also in the highest potential amount of released oil across the evaluated scenarios (between 0.15 and 0.26 g).

The previous results and analysis demonstrate that the proposed methods to assess the healing activation potential of the capsules are effective to provide design guidelines regarding the

type and amount of capsules required to increase the chances of initiating self-healing processes within these mixtures.

7. Summary and Conclusions

This computational study evaluated the mechanical response of self-healing asphalt mixtures with polynuclear capsules using FE modelling. The dynamic axial modulus |(E^*|) of randomly generated 2D microstructures of mixtures with no capsules and with 1.5 and 2.5 mm diameter capsules, added at 0.5 and 1.0% by the total weight, was quantified. Also, two approaches were proposed to compute the maximum theoretical number of capsules that could be activated under specific loading conditions and the corresponding potential amount of available healing agent in the mixture. The methods were illustrated through a compressive monotonic test, similar to those used in existing experimental efforts. To attain the objectives of the study, a total of 100 computational simulations were performed and different advanced post-processing methods were developed and implemented.

The main conclusions are:

- The dynamic axial modulus of the self-healing asphalt mixtures is not significatively affected by the addition of the capsules evaluated. This also suggests that the rutting resistance would not get compromised during the initial stage of the service life of the studied mixtures.

- The mixtures with 1.5 mm capsules were identified as an interesting alternative to design these self-healing asphalt mixtures, as they showed high activation potential indices, a higher number of capsules with activation potential (i.e., more probable activation points in the mixtures), and a higher amount of available healing agent. In fact, the mixture with 1.5 mm capsules added at 1.0% by total weight had the highest amount of available oil, and this value was between 1.4 and 2.0 times higher than in the mixture with 2.5 mm capsules added at the same addition dose. Among the cases studied, this design has the highest potential to promote self-healing.

- The impact of the inherent heterogeneity of the mixtures, measured through the COV among the 10 tested replicates for each case, was small in the case of the dynamic modulus

and moderate in the total amount of available oil. This means that if the volumetrics are controlled during the fabrication of the mixtures: i) the addition of capsules does not increase the uncertainty in the mechanical response of the material, and ii) the actual healing potential could be impacted at certain level due to the specific internal geometric characteristics of the microstructure of the mixture (i.e., uncertainty in the potential activation induced by the heterogeneity of the microstructure).

Although additional work to quantify the healing capability of the mixtures is required, the numerical results show that these mixtures have high activation potential, which is the first requirement to initiate internal self-healing processes. Future computational efforts include the development of new models to estimate the healing capacity of mixtures with micro-cracks in the mortar phase. Additionally, new and improved experimental efforts are needed to quantify the actual self-healing capacity of asphalt mortars and asphalt mixtures fabricated with these capsules under multiple realistic field conditions.

8. Acknowledgments

The authors are grateful to Mr. Fernando Paipilla and Ms. Fiorella Verbel for their support in the computation calibration activities conducted as part of this work.

9. References

Abu Al-Rub, R. K., Darabi, M. K., Little, D. N., & Masad, E. A. (2010). A micro-damage healing model that improves prediction of fatigue life in asphalt mixes. *International Journal of Engineering Science*, *48*(11), 966–990. https://doi.org/10.1016/j.ijengsci.2010.09.016

Aguirre, M. A., Hassan, M. M., Shirzad, S., Mohammad, L. N., Cooper, S., & Negulescu, I. I. (2017). Laboratory testing of self-healing microcapsules in asphalt mixtures prepared with recycled asphalt shingles. *Materials in Civil Engineering*, *29*(9). https://doi.org/10.1061/(ASCE)MT.1943-5533.0001942

Al-Mansoori, T., Micaelo, R., Artamendi, I., Norambuena-Contreras, J., & Garcia, A. (2017). Microcapsules for self-healing of asphalt mixture without compromising mechanical performance. *Construction and Building Materials*, *155*, 1091–1100. https://doi.org/10.1016/j.conbuildmat.2017.08.137

Al-Mansoori, T., Norambuena-Contreras, J., & Garcia, A. (2018). Effect of capsule addition and healing temperature on the self-healing potential of asphalt mixtures. *Materials and Structures/Materiaux et Constructions*, *51*(2). https://doi.org/10.1617/s11527-018-1172-5

Al-Mansoori, T., Norambuena-Contreras, J., Micaelo, R., & Garcia, A. (2018). Self-healing of asphalt mastic by the action of polymeric capsules containing rejuvenators. *Construction and Building Materials*, *161*(February), 330–339. https://doi.org/10.1016/j.conbuildmat.2017.11.125

Anupam, B. R., Sahoo, U. C., & Chandrappa, A. K. (2022). A methodological review on self-healing asphalt pavements. *Construction and Building Materials*, *321*. https://doi.org/10.1016/j.conbuildmat.2022.126395

ASTM International. (1997). *Flexible pavement rehabilitation and maintenance* (P. S. Kandhal & M. Stroup-Gardiner, Eds.; 1st ed.). https://doi.org/10.1520/STP1348-EB

Ayar, P., Moreno-Navarro, F., & Rubio-Gámez, M. C. (2016). The healing capability of asphalt pavements: A state of the art review. *Journal of Cleaner Production*, *113*, 28–40. https://doi.org/10.1016/j.jclepro.2015.12.034

Biligiri, K. P., Kaloush, K., & Uzan, J. (2010). Evaluation of asphalt mixtures' viscoelastic properties using phase angle relationships. International Journal of Pavement Engineering, 11(2), 143–152. https://doi.org/10.1080/10298430903033354

Caro, S., Castillo, D., Darabi, M., & Masad, E. (2018). Influence of different sources of microstructural heterogeneity on the degradation of asphalt mixtures. International Journal of Pavement Engineering, 19(1), 9–23. https://doi.org/10.1080/10298436.2016.1149839

Castillo, D., Caro, S., Darabi, M., & Masad, E. (2015). Studying the effect of microstructural properties on the mechanical degradation of asphalt mixtures. *Construction and Building Materials*, *93*, 70–83. https://doi.org/10.1016/j.conbuildmat.2015.05.108

Castillo, D., Caro, S., Darabi, M., & Masad, E. (2017). Modelling moisture-mechanical damage in asphalt mixtures using random microstructures and a continuum damage formulation. Road Materials and Pavement Design, 18(1), 1–21. https://doi.org/10.1080/14680629.2016.1138880

Castillo, D., Caro, S., Darabi, M., & Masad, E. (2018). Influence of aggregate morphology on the mechanical performance of asphalt mixtures. *Road Materials and Pavement Design*, *19*(4), 972–991. https://doi.org/10.1080/14680629.2017.1283357

Câmara, G., Azevedo, N. M., & Micaelo, R. (2023). Impact of Rejuvenator-Modified Mastic on Asphalt Mixture Stiffness: Meso-Scale Discrete Element Method Approach. Buildings, 13(12). https://doi.org/10.3390/buildings13123023

Cheng, H., Wang, Y., Liu, L., & Sun, L. (2022). Effects of using different dynamic moduli on predicted asphalt pavement responses in mechanistic pavement design. Road Materials and Pavement Design, 23(8), 1860–1876. https://doi.org/10.1080/14680629.2021.1924842

Cheng, H., Wang, Y., Liu, L., Sun, L., Zhang, Y., & Yang, R. (2021). Estimating Tensile and Compressive Moduli of Asphalt Mixture from Indirect Tensile and Four-Point Bending Tests. Journal of Materials in Civil Engineering, 33(1). https://doi.org/10.1061/(asce)mt.1943-5533.0003476

Concha, J. L., Delgadillo, R., Arteaga-Pérez, L. E., Segura, C., & Norambuena-Contreras, J. (2023). Optimised Sunflower Oil Content for Encapsulation by Vibrating Technology as a Rejuvenating Solution for Asphalt Self-Healing. Polymers 2023, 15(6), 1578; https://doi.org/10.3390/polym15061578

Concha, J. L., Sáez-Gutierrez, M., & Norambuena-Contreras, J. (2024). Mechanical activation assisted of biobased encapsulated rejuvenators to promote asphalt self-healing. *Materials Today Communications*, *38*(June 2023). https://doi.org/10.1016/j.mtcomm.2023.107735

Concha, J. L., Viana-Sepulveda, A., Caro, S., Arteaga-Pérez, L. E., & Norambuena-Contreras, J. (2024). Dynamic mechanical analysis of asphalt mortar samples containing millimetre-size capsules for self-healing purposes. *Powder Technology*, *440*(April). https://doi.org/10.1016/j.powtec.2024.119735

Espinosa, L., Caro, S., & Wills, J. (2020). Study of the influence of the loading rate on the fracture behaviour of asphalt mixtures and asphalt mortars. *Construction and Building Materials*, *262*, 120037. https://doi.org/10.1016/j.conbuildmat.2020.120037

Fabrizio, M., & Morro, A. (1987). *Mathematical Problems in Linear Viscoelasticity* (Society for Industrial and Applied Mathematics, Ed.). Society for Industrial and Applied Mathematics.

FEHRL. (2008). *New road construction concepts (NR2C); towards reliable, green, safe & smart, and human infrastructure in Europe*. Forum of European National Highway Research Laboratories (FEHRL) European Commission. https://www.fehrl.org/

Gallego, J., Del Val, M. A., Contreras, V., & Páez, A. (2013). Heating asphalt mixtures with microwaves to promote self-healing. *Construction and Building Materials*, *42*, 1–4. https://doi.org/10.1016/j.conbuildmat.2012.12.007

Garcia, A., Austin, C. J., & Jelfs, J. (2016). Mechanical properties of asphalt mixture containing sunflower oil capsules. *Journal of Cleaner Production*, *118*, 124–132. https://doi.org/10.1016/j.jclepro.2016.01.072

Garcia, A., Jelfs, J., & Austin, C. J. (2015). Internal asphalt mixture rejuvenation using capsules. *Construction and Building Materials*, *101*, 309–316. https://doi.org/10.1016/j.conbuildmat.2015.10.062

Gilabert, F. A., Garoz, D., & Van Paepegem, W. (2015). Stress concentrations and bonding strength in encapsulation-based self-healing materials. *Materials and Design*, *67*, 28–41. https://doi.org/10.1016/j.matdes.2014.11.012

Gonzalez-Torre, I., & Norambuena-Contreras, J. (2020). Recent advances on self-healing of bituminous materials by the action of encapsulated rejuvenators. *Construction and Building Materials*, *258*. https://doi.org/10.1016/j.conbuildmat.2020.119568

Hou, Y., Wang, L., Pauli, T., & Sun, W. (2015). Investigation of the Asphalt Self-Healing Mechanism Using a Phase-Field Model. *Journal of Materials in Civil Engineering*, *27*(3), 1–13. https://doi.org/10.1061/(asce)mt.1943-5533.0001047

Hussain, F., Ali, Y., & Irfan, M. (2021). Alternative Approach for Predicting the Phase Angle Characteristics of Asphalt Concrete Mixtures Based on Recurrent Neural Networks. Journal of Materials in Civil Engineering, 33(9). https://doi.org/10.1061/(asce)mt.1943-5533.0003855

Inozemtcev, S., Jelagin, D., Korolev, E., Fadil, H., Partl, M. N., & Do Trong, T. (2022). Experimental and numerical study on SMA modified with an encapsulated polymeric healing agent. *Materials and Structures/Materiaux et Constructions*, *55*(9). https://doi.org/10.1617/s11527-022-02059-8

Islam, M. R., & Tarefder, R. A. (2020). Chapter 8. Distresses in Flexible Pavement. In McGraw-Hill Education (Ed.), *Pavement Design: Materials, Analysis, and Highways* (1st ed.).

Karakaş, A. S., Sayin, B., & Kuloılu, N. (2014). The changes in the mechanical properties of neat and SBS-modified HMA pavements due to traffic loads and environmental effects over a one-year period. *Construction and Building Materials*, *71*, 406–415. https://doi.org/10.1016/j.conbuildmat.2014.08.060

Kargari, A., Arabani, M., & Mirabdolazimi, S. M. (2022). Effect of palm oil capsules on the self-healing properties of aged and unaged asphalt mixtures gained by resting period and microwave heating. *Construction and Building Materials*, *316*(November 2021), 125901. https://doi.org/10.1016/j.conbuildmat.2021.125901

Karki, P. (2010). *Computational and Experimental Characterization of Bituminous Composites Based on Experimentally Determined*. 131. http://digitalcommons.unl.edu/cgi/viewcontent.cgi?article=1003&context=civilengdiss

Kim, Y.-R., Allen, D. H., & Little, D. N. (2005). Damage-induced modeling of asphalt mixtures through computational micromechanics and cohesive zone fracture. *Journal of Materials in Civil Engineering*, *17*(5), 477–484. https://doi.org/10.1061/(asce)0899-1561(2005)17:5(477)

Lavin, P. G. (2003). *Asphalt pavements: a practical guide to design, production and maintenance for engineers and architects*: Taylor & Francis Group (Spone Press), Ed.; 1st ed. New York, USA.

Liang, B., Lan, F., Shi, K., Qian, G., Liu, Z., & Zheng, J. (2021). Review on the self-healing of asphalt materials: Mechanism, affecting factors, assessments and improvements. *Construction and Building Materials*, *266*, 120453. https://doi.org/10.1016/j.conbuildmat.2020.120453

Liu, Q., García, Á., Schlangen, E., & Ven, M. Van De. (2011). Induction healing of asphalt mastic and porous asphalt concrete. *Construction and Building Materials*, *25*(9), 3746–3752. https://doi.org/10.1016/j.conbuildmat.2011.04.016

Magnanimo, V., Huerne, H. L. ter, & Luding, S. (2012). Asphalt Durability and Self-healing Modelling with Discrete Particles Approach. In *7th RILEM International Conference on Cracking in Pavements* (pp. 1103–1114).

Maiti, S., Shankar, C., Geubelle, P. H., & Kieffer, J. (2006). Continuum and molecular-level modeling of fatigue crack retardation in self-healing polymers. *Journal of Engineering Materials and Technology*, *128*(4), 595–602. https://doi.org/10.1115/1.2345452

Manrique-Sanchez, L., Caro, S., & Arámbula-Mercado, E. (2018). Numerical modelling of ravelling in porous friction courses (PFC). Road Materials and Pavement Design, 19(3), 668–689. https://doi.org/10.1080/14680629.2016.1269661

Manrique-Sanchez, L., Caro, S., Estrada, N., Castillo, D., & Alvarez, A. E. (2022). Random generation of 2D PFC microstructures through DEM gravimetric methods. *Road Materials and Pavement Design*, *23*(4), 925–941. https://doi.org/10.1080/14680629.2020.1860804

Mauludin, L. M., & Oucif, C. (2018). Interaction between matrix crack and circular capsule under uniaxial tension in encapsulation-based self-healing concrete. *Underground Space (China)*, *3*(3), 181–189. https://doi.org/10.1016/j.undsp.2018.04.004

Mauludin, L. M., & Oucif, C. (2019). Modeling of self-healing concrete: A review. *Journal of Applied and Computational Mechanics*, *5*(Special Issue 3), 526–539. https://doi.org/10.22055/jacm.2017.23665.1167

Mauludin, L. M., & Rabczuk, T. (2021). Computational modeling of fracture in capsule-based self-healing concrete: A 3D study. *Frontiers of Structural and Civil Engineering*, *15*(6), 1337–1346. https://doi.org/10.1007/s11709-021-0781-1

Mauludin, L. M., Zhuang, X., & Rabczuk, T. (2018). Computational modeling of fracture in encapsulation-based self-healing concrete using cohesive elements. *Composite Structures*, *196*(April), 63–75. https://doi.org/10.1016/j.compstruct.2018.04.066

Micaelo, R., Al-Mansoori, T., & Garcia, A. (2016). Study of the mechanical properties and self-healing ability of asphalt mixture containing calcium-alginate capsules. *Construction and Building Materials*, *123*(July), 734–744. https://doi.org/10.1016/j.conbuildmat.2016.07.095

Micaelo, R., Freire, A. C., & Pereira, G. (2020). Asphalt self-healing with encapsulated rejuvenators: effect of calcium-alginate capsules on stiffness, fatigue and rutting properties. *Materials and Structures/Materiaux et Constructions*, *53*(1), 1–17. https://doi.org/10.1617/s11527-020-1453-7

Norambuena-Contreras, J., Arteaga-Pérez, L. E., Concha, J. L., & Gonzalez-Torre, I. (2021). Pyrolytic oil from waste tyres as a promising encapsulated rejuvenator for the extrinsic self-healing of bituminous materials. *Road Materials and Pavement Design*, *22*(S1), S117–S133. https://doi.org/10.1080/14680629.2021.1907216

Norambuena-Contreras, J., Arteaga-Perez, L. E., Guadarrama-Lezama, A. Y., Briones, R., Vivanco, J. F., & Gonzalez-Torre, I. (2020). Microencapsulated bio-based rejuvenators for the self-healing of bituminous materials. *Materials*, *13*(6). https://doi.org/10.3390/ma13061446

Norambuena-Contreras, J., Concha, J., Arteaga-Pérez, L., & Gonzalez-Torre, I. (2022). Synthesis and Characterisation of Alginate-Based Capsules Containing Waste Cooking Oil for Asphalt Self-Healing. *Applied Sciences*, *12*(5), 2739. https://doi.org/10.3390/app12052739

Norambuena-Contreras, J., & Garcia, A. (2016). Self-healing of asphalt mixture by microwave and induction heating. *Materials and Design*, *106*, 404–414. https://doi.org/10.1016/j.matdes.2016.05.095

Norambuena-Contreras, J., Liu, Q., Zhang, L., Wu, S., Yalcin, E., & Garcia, A. (2019). Influence of encapsulated sunflower oil on the mechanical and self-healing properties of dense-graded asphalt mixtures. *Materials and Structures/Materiaux et Constructions*, *52*(4), 1–13. https://doi.org/10.1617/s11527-019-1376-3

Norambuena-Contreras, J., Yalcin, E., Garcia, A., Al-Mansoori, T., Yilmaz, M., & Hudson-Griffiths, R. (2018). Effect of mixing and ageing on the mechanical and self-healing properties of asphalt mixtures containing polymeric capsules. *Construction and Building Materials*, *175*, 254–266. https://doi.org/10.1016/j.conbuildmat.2018.04.153

Norambuena-Contreras, J., Yalcin, E., Hudson-Griffiths, R., & Garcia, A. (2019). Mechanical and self-healing properties of stone mastic asphalt containing encapsulated rejuvenators. *Journal of Materials in Civil Engineering*, *31*(5), 04019052. https://doi.org/10.1061/(asce)mt.1943-5533.0002687

Norambuena-Contreras, J., Concha, J.L., Valdes-Vidal, G. *et al.* Optimised biopolymer-based capsules for enhancing the mechanical and self-healing properties of asphalt mixtures. *Mater Struct* **57**, 236 (2024). https://doi.org/10.1617/s11527-024-02508-6

Pauli, A. T. (2014). *Chemomechanics of Damage Accumulation and Damage-Recovery Healing in Bituminous Asphalt Binders*. Adam Tory Pauili & Sieca Repro. Delft, The Netherlands.

Rahman, A. S. M. A., & Tarefder, R. A. (2018). Viscosity-Based Complex Modulus and Phase-Angle Predictive Models for the Superpave Asphalt Mixtures of New Mexico. Journal of Materials in Civil Engineering, 30(3), 1–9. https://doi.org/10.1061/(asce)mt.1943-5533.0002202

Rhim, J. W. (2004). Physical and mechanical properties of water resistant sodium alginate films. *LWT - Food Science and Technology*, *37*, 323–330. https://doi.org/10.1016/j.lwt.2003.09.008

Roberts, F. L., Kandhal, P. S., Brown, E. R., Lee, D.-Y., Kennedy, T. W., & National Asphalt Pavement Association (NAPA). (1996). *Hot mix asphalt materials, mixture design and construction* ((NAPA) E. Foundation, Ed.; 2nd ed.). Lanham, Maryland, USA.

Romero, S., & Caro, S. (2019). *Evaluación del impacto mecánico de la adición de RAP en mezclas asfálticas en caliente usando un modelo de mecánica computacional (Master Thesis)* [Universidad de los Andes, Bogotá DC, Colombia]. https://doi.org/10.25100/iyc.v16i1.3707

Su, J. F., Qiu, J., & Schlangen, E. (2013). Stability investigation of self-healing microcapsules containing rejuvenator for bitumen. *Polymer Degradation and Stability*, *98*(6), 1205–1215. https://doi.org/10.1016/j.polymdegradstab.2013.03.008

Sun, D., Li, B., Tian, Y., Lu, T., Zhu, X., Sun, G., & Gilabert, F. A. (2019). Aided regeneration system of aged asphalt binder based on microcapsule technology. *Construction and Building Materials*, *201*, 571–579. https://doi.org/10.1016/j.conbuildmat.2018.12.167

Tabaković, A., & Schlangen, E. (2016). Self-healing technology for asphalt pavements. *Advances in Polymer Science*, *273*, 285–306. https://doi.org/10.1007/978-3-319-32778-5

Viana-Sepulveda, A., Caro, S., Concha, J. L., & Norambuena-Contreras, J. (2023). Rheological properties characterization of self-healing asphalt mortars. In *Airfield and Highway Pavements 2023 (ASCE)*. (pp. 130–138).

768 Walls, J., & Smith, M. R. (1998). *Life-cycle cost analysis in pavement design (FHWA-SA-98-079)* (Issue
769 September). https://doi.org/10.1007/978-94-007-2724-3_6

770 Wang, Y. Y., Tan, Y. Q., Lv, H. J., & Han, M. Z. (2022). Evaluation of rheological and self-healing properties of
771 asphalt containing microcapsules modified with graphene. *Construction and Building Materials*, *357*(October),
772 129287. https://doi.org/10.1016/j.conbuildmat.2022.129287

773 Weijermars, R. (1997). Chapter 5: Elasticity. In Principles of Rock Mechanics (pp. 65–78). Alboran Science Pub.

774 Xiang, L. Y., Mohammed, M. A., & Samsu Baharuddin, A. (2016). Characterisation of microcrystalline cellulose
775 from oil palm fibres for food applications. *Carbohydrate Polymers*, *148*, 11–20.
776 https://doi.org/10.1016/j.carbpol.2016.04.055

777 Xu, S., Tabaković, A., Liu, X., Palin, D., & Schlangen, E. (2019). Optimization of the calcium alginate capsules for
778 self-healing asphalt. *Applied Sciences (Switzerland)*, *9*(3). https://doi.org/10.3390/app9030468

779 Xu, S., Tabaković, A., Liu, X., & Schlangen, E. (2018). Calcium alginate capsules encapsulating rejuvenator as
780 healing system for asphalt mastic. *Construction and Building Materials*, *169*, 379–387.
781 https://doi.org/10.1016/j.conbuildmat.2018.01.046

782 Xue, B., Wang, H., Pei, J., Li, R., Zhang, J., & Fan, Z. (2017). Study on self-healing microcapsule containing
783 rejuvenator for asphalt. *Construction and Building Materials*, *135*, 641–649.
784 https://doi.org/10.1016/j.conbuildmat.2016.12.165

785 Yamaç, Ö. E., Yilmaz, M., Yalçın, E., Kök, B. V., Norambuena-Contreras, J., & Garcia, A. (2021). Self-healing of
786 asphalt mastic using capsules containing waste oils. *Construction and Building Materials*, *270*.
787 https://doi.org/10.1016/j.conbuildmat.2020.121417

788 Yan Li, P. H., & Zhang, M. (2021). Fabrication, characterization and assessment of the capsules containing
789 rejuvenator for improving the self-healing performance of asphalt materials: A review. *Journal of Cleaner*
790 *Production*, *287*. https://doi.org/https://doi.org/10.1016/j.jclepro.2020.125079.

791 Zhang, H., Bai, Y., & Cheng, F. (2018). Rheological and self-healing properties of asphalt binder containing
792 microcapsules. *Construction and Building Materials*, *187*, 138–148.
793 https://doi.org/10.1016/j.conbuildmat.2018.07.172

794 Zhang, L., Liu, Q., Li, H., Norambuena-Contreras, J., Wu, S., Bao, S., & Shu, B. (2019). Synthesis and
795 characterization of multi-cavity Ca-alginate capsules used for self-healing in asphalt mixtures. *Construction*
796 *and Building Materials*, *211*, 298–307. https://doi.org/10.1016/j.conbuildmat.2019.03.224

797 Ziari, H., Amiri, E. N., & Ayar, P. (2023). Investigation of the combination of microwave heating and calcium
798 alginate capsule rejuvenation healing methods for cold mix asphalt considering the type of compaction effort.
799 *Construction and Building Materials*, *407*(September), 133437.
800 https://doi.org/10.1016/j.conbuildmat.2023.133437